Conference on Modelling Fluid Flow (CMFF'22)
The 18th International Conference on Fluid Flow Technologies
Budapest, Hungary, August 30-September 2, 2022

DYNAMICS OF HIGH-SPEED DROP IMPACT ON DEEP LIQUID POOL

Hui WANG[1], Shuo LIU[2], Annie-Claude BAYEUL-LAINÉ[3], Olivier COUTIER-DELGOSHA[4]

[1] Corresponding Author. Univ. Lille, CNRS, ONERA, Arts et Metiers Institute of Technology, Centrale Lille, UMR 9014 - LMFL - Laboratoire de Mécanique des Fluides de Lille - Kampé de Fériet, F-59000 Lille, France. Tel.: +33 06 08 10 25 28, E-mail: hui.wang@ensam.eu
[2] Univ. Lille, CNRS, ONERA, Arts et Metiers Institute of Technology, Centrale Lille, UMR 9014 - LMFL - Laboratoire de Mécanique des Fluides de Lille - Kampé de Fériet, F-59000 Lille, France. E-mail: shuo.liu@ensam.eu
[3] Univ. Lille, CNRS, ONERA, Arts et Metiers Institute of Technology, Centrale Lille, UMR 9014 - LMFL - Laboratoire de Mécanique des Fluides de Lille - Kampé de Fériet, F-59000 Lille, France. E-mail: annie-claude.bayeul-laine@ensam.eu
[4] Univ. Lille, CNRS, ONERA, Arts et Metiers Institute of Technology, Centrale Lille, UMR 9014 - LMFL - Laboratoire de Mécanique des Fluides de Lille - Kampé de Fériet, F-59000 Lille, France. E-mail: olivier.coutier-delgosha@ensam.eu

ABSTRACT

In this work, high-speed drop impact onto deep volume of the same liquid is numerically studied in 3D using Direct Numerical Simulation (DNS). The numerical results are compared with the previous experimental works by Murphy et al. [1]. Most of the distinctive features during the impact, including the evolution of the crown and cavity, the ligaments emanating from the rim of the crown, the formation of the bubble canopy, the central spiral jet that pierces through the bottom of the cavity and the subsequent broad upward jet, are correctly reproduced. The trajectory of the upper rim of the crown as well as the depth and width of the subsurface cavity are tracked during the simulation. Very reliable quantitative agreements between numerical and experimental data are obtained with respect to the time evolution of the crown rim and cavity dimensions. The simulation shows very good qualitative and quantitative agreement against the available experimental data, which enables the further investigation of the internal mechanisms of drop impact in the future.

Keywords: bubble canopy, crown and cavity, Direct Numerical Simulation, high-speed drop impact, splashing

NOMENCLATURE

H	$[m]$	computational pool depth
L	$[m]$	computational size of domain
P	$[Pa]$	pressure field
d	$[m]$	drop diameter
f	$[-]$	volume fraction
u_0	$[m/s]$	initial impacting speed
$\underline{U}$	$[m/s]$	velocity field
$\underline{\underline{D}}$	$[-]$	deformation tensor
$\underline{a}$	$[m/s^2]$	body force
$\underline{g}$	$[m/s^2]$	gravity
$\underline{n}$	$[-]$	unit vector normal to the interface
δ	$[m]$	initial gap between drop and pool
κ	$[m^{-1}]$	curvature
μ	$[Pa \cdot s]$	dynamic viscosity
ρ	$[kg/m^3]$	density
σ	$[N/m]$	surface tension coefficient

Subscripts and Superscripts

h, v	horizontal and vertical direction
w, a	water phase, air phase

1. INTRODUCTION

The process of drop impact is widely observed in nature and involves many fascinating physical phenomena, but challenging for further studying due to the increased complexity of multi-scale flows and interfacial dynamics [2]. Knowing from daily shower, natural rainfall, soil erosion [3, 4], industrial spray injecting&cooling [5, 6] and agriculture irrigation [7], drop impact exists ubiquitously in our life. Scientific research on uncovering the internal mechanisms of drop impact thus shows huge potential in facilitating the technical applications in various areas where this process is involved.

Since the path-breaking works started more than a century ago [8], various studies of drop impact have been initiated afterwards. Different scenarios of drop impact regarding to liquid [9, 10] or solid target [11, 12], shallow [13, 14] or deep pool [15, 16], miscible [17] or immiscible [18] liquids have been discussed. For drop impact on deep pool, three dimensionless parameters are usually used to describe the splashing, namely Reynolds number $Re = \rho u_0 d/\mu$, Weber number $We = \rho u_0^2 d/\sigma$ and Froude number

$Fr = u_0^2/gd$, where ρ is liquid density, u_0 is initial impacting speed, d is drop diameter, $\underline{g}$ is gravity, μ and σ are viscosity and surface tension. In order to uncover the underlying flow physics, multiple aspects of drop impact such as the behaviour of initial liquid sheet [16, 19, 20, 21], air bubble entrainment [22, 23], evolution of crown and cavity [14, 24, 25], as well as the formation of secondary droplets [1, 26] have been broadly investigated.

In the most recent works, attention has been especially focused on the first stages of impact, where the liquid sheet is ejected from the neck and the entrapped air layer under the droplet is ruptured, resulting in the splashing of very fine spray [19, 27] and the generation of secondary bubbles [28, 22, 23], but the mechanisms are still not well elucidated. Additionally, the non-axisymmetric behaviors of vortex shedding and the observed ejecta behaviour from bottom visualizations in cases of impacts on thin films [29] show that these phenomena break the axisymmetry at fine scale, and may be related to three-dimensional mechanisms. This clearly poses a new challenge to numerical studies, which mostly assume axisymmetry [21, 30]

As for later stages of the impact, qualitatively different regimes of phenomenon have been categorized [31, 32, 33, 34] at relatively small range of Re and We numbers, depending on various impacting conditions. For the most energetic regime of drop impact with higher impacting speed and larger drop diameter, the interfical dynamics can be significantly modified. As schemed by Engel [15], after the first stage of splashing, the liquid sheet expands radially and forms a thin-walled 'crown' above the surface of the target pool. Next, the rim of the crown rises to a maximum position and then closes up into a "bubble canopy" followed by a central liquid jet, trapping a volume of air inside. In this process, ligaments emanate from the rim of crown and eject a great number of fine droplets to the air upwards and outwards. Such tiny airborne droplets may raise potential health issues to the public under certain circumstances [1].

Numerical approaches have been employed to the analysis of drop impact since decades. Both axisymmetric [35, 14, 36, 32, 30] and three dimensional [37, 38, 39] simulations can be found in literature, using mostly DNS approaches. For three-dimension calculations, whose primary objective is to capture the non-axisymmetric mechanisms involved in the splashing. Efforts are focused on dynamic refinement techniques [40, 41], in order to resolve the multiple interfaces resulting from the splashing, while ensuring a reasonable grid size. In the latter study, the authors show that a minimum cell size of about 50 to 100 μm is sufficient to capture most of the features of the splash. However, that conclusion was drawn for Weber numbers around 250, so it may not directly apply to the configuration investigated in the present study.

In this work, we perform three-dimensional direct numerical simulation (DNS) of high-speed drop impact on deep liquid pool. The paper is organized as follows: the numerical approaches are described in Section 2, the flow configurations and numerical parameters are explained in Section 3, the numerical results are demonstrated and discussed in Section 4 and the paper is summarized in Section 5.

2. NUMERICAL APPROACHES

2.1. Governing equations

The drop impact of gas-liquid system is considered as incompressible flows, and it solves a system of the mass balance equation Eq. (1), the momentum balance equation Eq. (2) and the advection of one-fluid formulation Eq. (3), called hereafter the color function.

$$\nabla \cdot \underline{U} = 0 \tag{1}$$

$$\rho\left(\frac{\partial \underline{U}}{\partial t} + (\underline{U}\cdot\nabla)\underline{U}\right) = -\nabla P + \nabla\cdot(\mu\underline{\underline{D}}) + \rho\underline{a} + \sigma\kappa\delta_s\underline{n} \tag{2}$$

$$\frac{\partial f}{\partial t} + \nabla\cdot(f\underline{U}) = 0 \tag{3}$$

Where $\underline{U}$ the velocity field, ρ the density, P the pressure, μ the viscosity, $\underline{\underline{D}}$ the deformation tensor, $\underline{a}$ the body force along the impacting direction. The last term in Eq. (2) is the surface tension force, with κ the curvature of the interface, σ the surface tension coefficient which is taken as constant in the present study, and $\underline{n}$ the unit vector normal to the interface. This term is zero everywhere but at the liquid/gas interface, as controlled by the Dirac function δ_s. The volume fraction f is transported by color function in Eq. (3).

2.2. Numerical solver

We use the open source Basilisk framework [42] to simulate the process of drop impact. The momentum-conserving volume-of-fluid (MCVOF) numerical scheme, introduced by Fuster & Popinet [43], is employed here to simulate the problem of two-phase flow. The color function (Eq. (3)) is solved based on a volume fraction advection scheme proposed in [44], which exhibits the complete mass conservation and makes it ideal for highly energetic free-surface flows. The interface then can be represented using Piecewise Linear Interface Capturing (PLIC) VOF method [45]. For Eq. (2), the Crank–Nicholson discretization of the viscous terms is second order accurate in time and unconditionally stable, while the convective terms are computed using the Bell-Colella-Glaz (BCG) second order unsplit upwind scheme [46], which is stable for CFL numbers smaller than one. The surface tension is

calculated using the continuum surface force (CSF) model described in [47].

The tree-based structure [48] of the spatial discretization is applied to adaptively follow the smallest structures of flow, thus concentrating the computational effort on the area where it is most needed. Starting from a root cell so called "parent"cell at level 0, eight "children" cells will be generated in 3D at level 1 (four "children" in 2D). With the maximum level of refinement n, the finest resolution will be 2^n in each dimension, and various level of local refinement can be presented in the spatial domain at the same time.

Basilisk employs the Adaptive Mesh Refinement (AMR) [49] to adaptively refine/coarsen the grids based on the wavelet-estimated numerical error of the local dynamics, which makes it especially appropriate for the present application where multiple interfaces and numerous droplets and bubbles are expected. The resolution will be adapted every time step according to the estimated discretization error of the spatially-discretized fields (volume fraction, velocity, curvature..). The grid will be refined as long as the wavelet-estimated error exceeds the given threshold, which eventually leads to a multi-level spatial resolution from minimum level L_{min} to maximum level L_{max} over the domain.

The great superiority of parallel capacity and computational efficiency of Basilisk code are discussed in [50]. The capabilities of Basilisk solver have been extensively validated on various problems for multi-phase complex flows here [42].

3. NUMERICAL PARAMETERS

In this work, we reproduce one specific case of high-speed drop impact that was discussed in [1] as a control case for the study of raindrop impact onto oil slick. We use the artificial seawater here for both the drop and pool, since the properties of the liquids are almost the same. The surrounding gas is air. The density and viscosity ratios between seawater and air are $\rho_w/\rho_a = 1018$ and $\mu_w/\mu_a = 180$. The drop is defined as an oblate ellipsoid with horizontal and vertical diameters $d_h = 0.0043m$ and $d_v = 0.0038m$ respectively, which leads to an average diameter $d \approx 0.004m$. The terminal speed of the drop before impact is $u_0 = 7.2m/s$.

As shown in Figure 1, the drop is initialized above the free surface of the liquid pool and the computational domain is a cubic with a side length $L = 16d$. The initial undisturbed surface of pool is located in the middle of the vertical direction, thus the depth of the pool is $H = 8d$, which ensures enough space for the growth of crown and cavity as well as avoids any wall effects from boundaries. The initial gap between drop and pool is $\delta = 0.1d$, allowing the observation of air sheet entrainment near the contact line. The free outflow boundary conditions are imposed on the top of the domain, while the symmetry boundary conditions are applied by default for other boundaries.

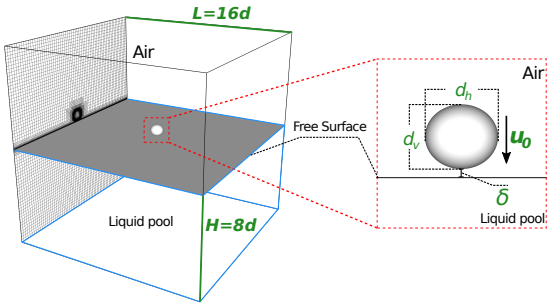

Figure 1. Initial numerical configurations of three-dimensional simulation. The left panel shows the overall computational domain and the initial mesh refinement at a plane cross the center of drop. The right panel shows a zoomed-in view near the drop

At the initial time, it is expected to refine the mesh with a higher level in the vicinity of the drop and free surface as shown in Fig.1, and the mesh is coarser gradually away from the interface. This will give a promising geometric description of the drop and free surface at the beginning and lower the RAM requirement for initialization. Once the simulation starts, the mesh will be redistributed adaptively based on the AMR algorithm using the volume fraction field with tolerance $fErr = 7e-4$ and the velocity field with tolerance $uErr = 1e-1$ as adaption criteria .

We have carried out extensive tests to explore the effects of the minimum spatial resolution in comparison with experimental data. One finds that the dynamics of the early-time liquid sheet and the entrapped air bubble affects significantly the subsequent formation of the thin-walled crown and its closure at high Re and We numbers. Our preliminary study have shown that a grid resolution of at least 1024 cells per diameter is necessary to capture the correct regime of early splashing for the present work. This will need to apply a maximum level of refinement at $L_{max} = 14$, which corresponds to an equivalent uniform grid of more than 4.3 trillion $[(2^{14})^3]$ cells.

Based on the physical characteristics during the impact, we have divided the simulation into two consecutive stages, namely the early-time splashing stage when $t \leqslant 2ms$ (***S1***) and the later crown stage when $t > 2ms$ (***S2***). At stage ***S1***, very thin liquid sheet is ejected and interacts strongly with the surface of the drop&pool, and numerous very fine droplets and bubbles are formed, thus the primary objective would be to capture the flow dynamics near the contact region in finer scale. Figure 2 shows the mesh refinement strategy applied at initial stage. A higher maximum level $L_{max} = 14$ $(3.9\mu m)$ is used in the vicinity of the free surface to resolve the dy-

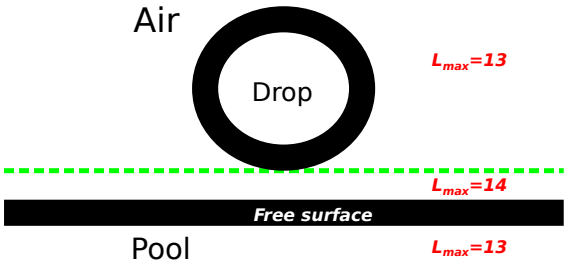

Figure 2. Mesh refinement strategy at stage *S*1. The region close to the free surface of the pool is calculated at higher maximum refinement (L_{max} = 14) for capturing the early-time dynamics of the very thin liquid sheet

namics of the liquid sheet in smaller scale, while L_{max} = 13 (7.8μm) is used for the rest of the domain to capture the statistics of droplets and bubbles. At stage ***S*2**, the crown has been developed and the rim of the crown is thickened due to the effect of surface tension. The secondary droplets shed from the top of the crown at this stage are generally in larger scales, comparing with the one from the initial stage. Therefore, we restart the simulation at $t = 2ms$ using the saved "dump" file from the initial stage with L_{max} = 12 (15.6μm) over the whole computational domain, which allows to capture the main physical dynamics of the crown and cavity till the end of the simulation ($t = 48ms$). This mesh refinement strategy ensures that the simulation is doable in a full three-dimensional configuration and can be accomplished in a "reasonable" time, in considering the available computational resources. The numerical results presented in section 4 were performed on 1024 cores for 33.5 days, which consumes more than 8.21×10^5 CPU-hours totally, using the computational resources on Advanced Research Computing (ARC) at Virginia Tech.

4. RESULTS

4.1. Phenomenology

Figure 3 shows the global evolution of high-energy drop impact during the 48ms after contact. The side-view of numerical results (bottom) are compared with experimental holograms (top) in time series. The time point of the contact is defined as t = 0. At t=-1ms, the drop is initialised above the surface of pool. Once the simulation starts, the drop will fall downwards to hit the pool driven by the combination of initial impacting speed and gravitational force. Directly after the impact (t=1ms), a cylindrical wave is generated around a flat-bottomed disk-like cavity due to the violent penetration of drop liquid. At this time, most of the drop liquid is concentrated on the bottom of the cavity and the submergence of the drop/pool interface can be approximated as half of the initial drop impacting velocity [51]. Next, the drop keeps expanding and spreads into a thin layer of

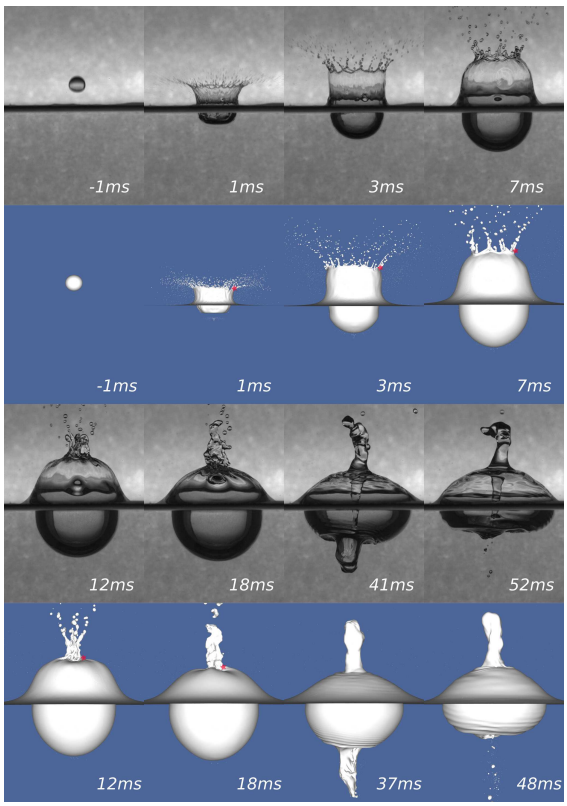

Figure 3. Qualitative comparisons between experimental and numerical results for high-speed drop impact. The red stars indicate the tracked positions of the crown rim

liquid that is distributed along the interior surface of the cavity, stretching the cavity into a typical hemispherical shape (t=3ms). By t=7ms, the orientation of the rim of ligament transitions from almost horizontal to vertical and the top of the crown starts to bend towards the center. At around t=12ms, the crown eventually closes up, trapping a volume of air inside. After the closure of the crown rim, a central spiral jet is then ejected vertically from the merging point and the downward moving jet eventually pierces the cavity bottom at t=37ms, which will result in the formation of a broad upward jet evidenced at t=48ms.

The qualitative comparison shows that our simulation reproduces all the distinctive features observed in the experiments. The correct prediction of the morphologic behavior of the air-water interface, the transition of ligaments orientation, and the exact time where the upper rim of the crown necks in and the central spiral jet pierces the cavity bottom are especially convincing. A general good agreement to the experiments is obtained.

4.2. Kinematics

For further validating our numerical strategy, the kinematic behaviors of the crown and cavity are extracted from numerical and experimental results.

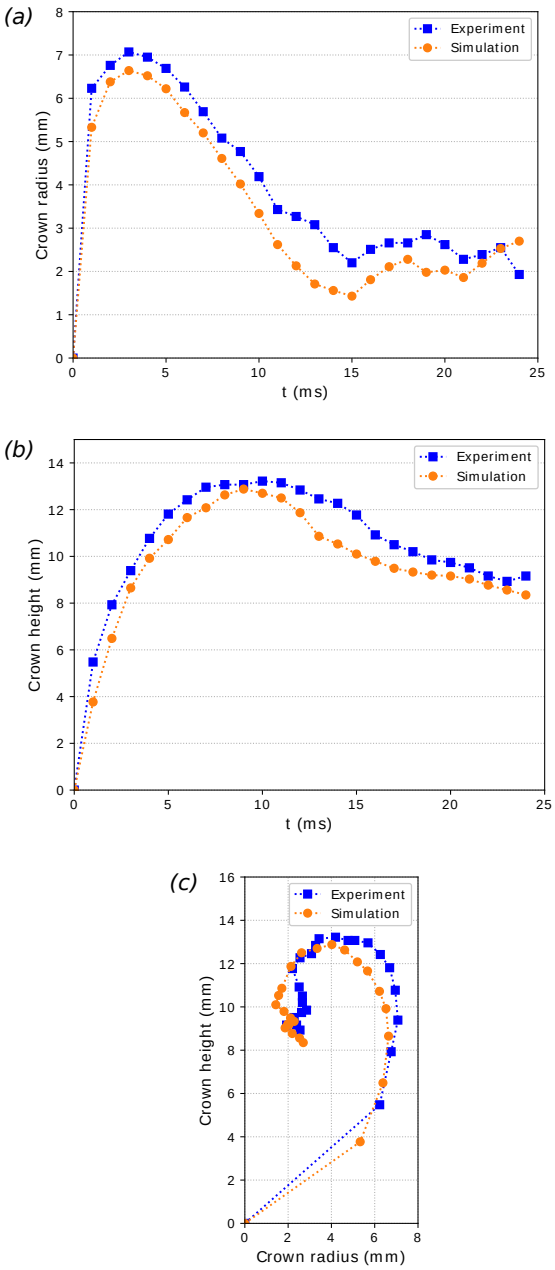

Figure 4. Analysis of the kinematic behaviours of the rim of the crown with time. The definition of the positions of the crown rim are marked as red stars in Fig. 3. (a) Radius of crown rim, (b) Height of crown rim and (c) Trajectory of crown rim

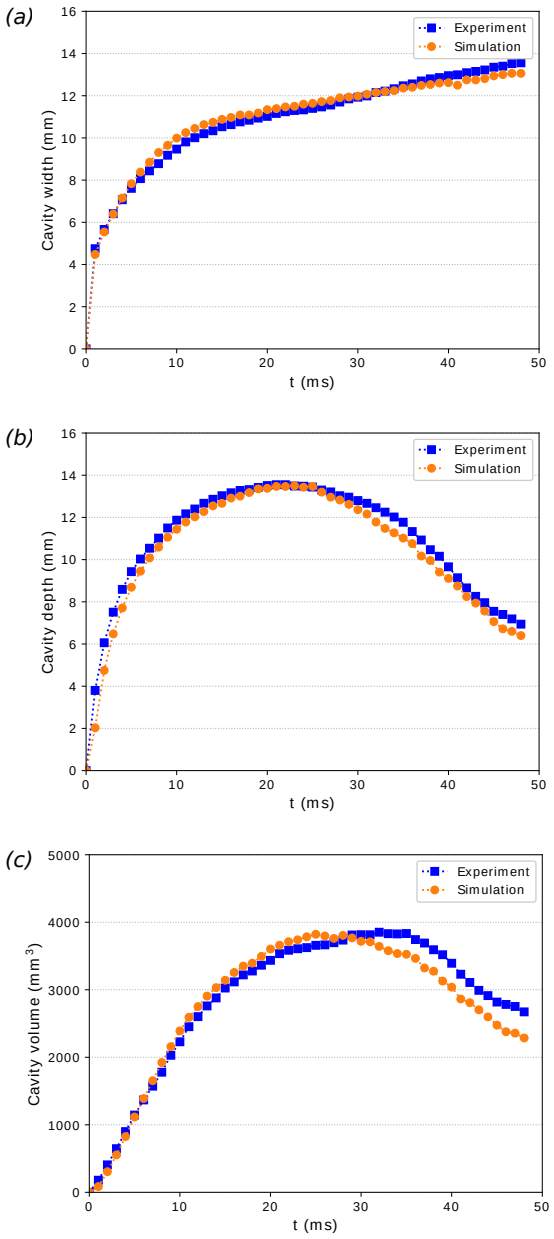

Figure 5. Analysis of the kinematic behaviours of the subsurface cavity with time. (a) Width of cavity, (b) Depth of cavity and (c) Volume of cavity

Figure 4 tracks the positions of the rim of the crown with time. The variation of the radius and height of the crown rim are shown in Fig. 4 (a) and (b), and the trajectory of the crown rim is then plotted in Fig. 4 (c). Below the initial free surface, the dimensions of the radially expanding cavity are also characterized by its width and depth in Figure 5 (a) and (b). The volume of the cavity thus is calculated as half of an ellipsoid in Fig. 5 (c).

Fig. 4 and 5 confirms this conclusion: both the trajectory of the edges of the upper rim and the dimensions of the subsurface cavity are also found in very good quantitative agreement with the experimental measurements.

5. SUMMARY

We present numerical investigation of the high-speed drop impact on deep liquid pool using direct numerical simulation. The full three-dimensional simulations are performed based on the Basilisk framework using volume of fluid and adaptive mesh refinement techniques. The simulations have been conducted in the exact same configuration described

in [1], for the purpose of a detailed comparison with available experimental data. It shows that our simulation successfully reproduced all the distinctive features observed in the experiments. We also found very good quantitative agreements between numerical and experimental results with respect to the trajectory of the crown rim, the cavity dimensions as well as the time point where the dome closes up and the central spiral jet pierces the cavity bottom. The rather good validation confirms the feasibility of the numerical scheme, which also enables to prepare in a future work an in-depth analysis of the internal physical mechanisms that is hard to be observed in the experiments.

ACKNOWLEDGEMENTS

This work has been supported by the scholarship from China Scholarship Council (CSC) under the Grant CSC NO. 201908320462.

REFERENCES

[1] Murphy, D. W., Li, C., d'Albignac, V., Morra, D., and Katz, J., 2015, "Splash behaviour and oily marine aerosol production by raindrops impacting oil slicks", *Journal of Fluid Mechanics*, Vol. 780, pp. 536–577.

[2] Deegan, R., Brunet, P., and Eggers, J., 2007, "Complexities of splashing", *Nonlinearity*, Vol. 21 (1), p. C1.

[3] Ekern, P. C., 1951, "Raindrop impact as the force initiating soil erosion", *Soil Science Society of America Journal*, Vol. 15 (C), pp. 7–10.

[4] Joung, Y. S., and Buie, C. R., 2015, "Aerosol generation by raindrop impact on soil", *Nature communications*, Vol. 6 (1), pp. 1–9.

[5] Kim, J., You, S., and Choi, S. U., 2004, "Evaporative spray cooling of plain and microporous coated surfaces", *International Journal of Heat and Mass Transfer*, Vol. 47 (14-16), pp. 3307–3315.

[6] Srikar, R., Gambaryan-Roisman, T., Steffes, C., Stephan, P., Tropea, C., and Yarin, A., 2009, "Nanofiber coating of surfaces for intensification of drop or spray impact cooling", *International Journal of Heat and Mass Transfer*, Vol. 52 (25-26), pp. 5814–5826.

[7] Yan, H., Bai, G., He, J., and Li, Y., 2010, "Model of droplet dynamics and evaporation for sprinkler irrigation", *Biosystems engineering*, Vol. 106 (4), pp. 440–447.

[8] Worthington, A. M., 1883, "On impact with a liquid surface", *Proceedings of the Royal Society of London*, Vol. 34 (220-223), pp. 217–230.

[9] Mukherjee, S., and Abraham, J., 2007, "Crown behavior in drop impact on wet walls", *Physics of fluids*, Vol. 19 (5), p. 052103.

[10] Guo, Y., Lian, Y., and Sussman, M., 2016, "Investigation of drop impact on dry and wet surfaces with consideration of surrounding air", *Physics of Fluids*, Vol. 28 (7), p. 073303.

[11] Josserand, C., and Thoroddsen, S. T., 2016, "Drop impact on a solid surface", *Annual review of fluid mechanics*, Vol. 48, pp. 365–391.

[12] Jian, Z., Josserand, C., Popinet, S., Ray, P., and Zaleski, S., 2018, "Two mechanisms of droplet splashing on a solid substrate", *Journal of Fluid Mechanics*, Vol. 835, pp. 1065–1086.

[13] Ferreira, A. G., and Singer, M. J., 1985, "Energy dissipation for water drop impact into shallow pools", *Soil Science Society of America Journal*, Vol. 49 (6), pp. 1537–1542.

[14] Berberović, E., van Hinsberg, N. P., Jakirlić, S., Roisman, I. V., and Tropea, C., 2009, "Drop impact onto a liquid layer of finite thickness: Dynamics of the cavity evolution", *Physical Review E*, Vol. 79 (3), p. 036306.

[15] Engel, O. G., 1966, "Crater depth in fluid impacts", *Journal of Applied Physics*, Vol. 37 (4), pp. 1798–1808.

[16] Thoroddsen, S., 2002, "The ejecta sheet generated by the impact of a drop", *Journal of Fluid Mechanics*, Vol. 451, pp. 373–381.

[17] Walker, T. W., Logia, A. N., and Fuller, G. G., 2015, "Multiphase flow of miscible liquids: jets and drops", *Experiments in Fluids*, Vol. 56 (5), pp. 1–14.

[18] Lhuissier, H., Sun, C., Prosperetti, A., and Lohse, D., 2013, "Drop fragmentation at impact onto a bath of an immiscible liquid", *Physical review letters*, Vol. 110 (26), p. 264503.

[19] Thoroddsen, S. T., Thoraval, M.-J., Takehara, K., and Etoh, T., 2011, "Droplet splashing by a slingshot mechanism", *Physical review letters*, Vol. 106 (3), p. 034501.

[20] Zhang, L., Toole, J., Fezzaa, K., and Deegan, R., 2012, "Evolution of the ejecta sheet from the impact of a drop with a deep pool", *Journal of Fluid Mechanics*, Vol. 690, pp. 5–15.

[21] Thoraval, M.-J., Takehara, K., Etoh, T. G., Popinet, S., Ray, P., Josserand, C., Zaleski, S., and Thoroddsen, S. T., 2012, "von Kármán vortex street within an impacting drop", *Physical review letters*, Vol. 108 (26), p. 264506.

[22] Thoroddsen, S., Etoh, T., and Takehara, K., 2003, "Air entrapment under an impacting drop", *Journal of Fluid Mechanics*, Vol. 478, pp. 125–134.

[23] Thoraval, M.-J., Takehara, K., Etoh, T., and Thoroddsen, S. T., 2013, "Drop impact entrapment of bubble rings", *Journal of Fluid Mechanics*, Vol. 724, pp. 234–258.

[24] Bisighini, A., Cossali, G. E., Tropea, C., and Roisman, I. V., 2010, "Crater evolution after the impact of a drop onto a semi-infinite liquid target", *Physical Review E*, Vol. 82 (3), p. 036319.

[25] Michon, G. J., Josserand, C., and Séon, T., 2017, "Jet dynamics post drop impact on a deep pool", *Physrevfluids*, Vol. 2 (2).

[26] Liu, X., 2018, "Experimental study of drop impact on deep-water surface in the presence of wind", *Journal of Physical Oceanography*, Vol. 48 (2), pp. 329–341.

[27] Zhang, L., Toole, J., Fezzaa, K., and Deegan, R., 2012, "Splashing from drop impact into a deep pool: multiplicity of jets and the failure of conventional scaling", *Journal of fluid mechanics*, Vol. 703, pp. 402–413.

[28] Pumphrey, H. C., and Elmore, P. A., 1990, "The entrainment of bubbles by drop impacts", *Journal of Fluid Mechanics*, Vol. 220, pp. 539–567.

[29] Li, E. Q., M.-J., T., Marston, J. O., and Thoroddsen, S. T., 2018, "Early azimuthal instability during drop impact", *Journal of Fluid Mechanics*, Vol. 848, pp. 821–835.

[30] Agbaglah, G., Thoraval, M.-J., Thoroddsen, S. T., Zhang, L. V., Fezzaa, K., and Deegan, R. D., 2015, "Drop impact into a deep pool: vortex shedding and jet formation", *J Fluid Mech*, Vol. 764, p. R1.

[31] Rein, M., 1996, "The transitional regime between coalescing and splashing drops", *Journal of Fluid Mechanics*, Vol. 306, pp. 145–165.

[32] Ray, B., Biswas, G., and Sharma, A., 2015, "Regimes during liquid drop impact on a liquid pool", *Journal of Fluid Mechanics*, Vol. 768, pp. 492–523.

[33] Gielen, M. V., Sleutel, P., Benschop, J., Riepen, M., Voronina, V., Visser, C. W., Lohse, D., Snoeijer, J. H., Versluis, M., and Gelderblom, H., 2017, "Oblique drop impact onto a deep liquid pool", *Physical review fluids*, Vol. 2 (8), p. 083602.

[34] Wu, Z., Hao, J., Lu, J., Xu, L., Hu, G., and Floryan, J. M., 2020, "Small droplet bouncing on a deep pool", *Physics of Fluids*.

[35] Morton, D., Rudman, M., and Jong-Leng, L., 2000, "An investigation of the flow regimes resulting from splashing drops", *Physics of Fluids*, Vol. 12 (4), pp. 747–763.

[36] Ervik, Å., Hellesø, S. M., Munkejord, S. T., and Müller, B., 2014, "Experimental and computational studies of water drops falling through model oil with surfactant and subjected to an electric field", *2014 IEEE 18th International Conference on Dielectric Liquids (ICDL)*, IEEE, pp. 1–6.

[37] Rieber, M., and Frohn, A., 1999, "A numerical study on the mechanism of splashing", *International Journal of Heat and Fluid Flow*, Vol. 20 (5), pp. 455–461.

[38] Brambilla, P., and Guardone, A., 2013, "Automatic tracking of corona propagation in three-dimensional simulations of non-normal drop impact on a liquid film", *Computing*, Vol. 95 (5), pp. 415–424.

[39] Shin, S., Chergui, J., and Juric, D., 2017, "A solver for massively parallel direct numerical simulation of three-dimensional multiphase flows", *Journal of Mechanical Science and Technology*, Vol. 31 (4), pp. 1739–1751.

[40] Nikolopoulos, N., Theodorakakos, A., and Bergeles, G., 2007, "Three-dimensional numerical investigation of a droplet impinging normally onto a wall film", *Journal of computational physics*, Vol. 225 (1), pp. 322–341.

[41] Brambilla, P., and Guardone, A., 2015, "Assessment of dynamic adaptive grids in volume-of-fluid simulations of oblique drop impacts onto liquid films", *Journal of Computational and Applied Mathematics*, Vol. 281, pp. 277–283.

[42] Popinet, S., and collaborators, 2013–2022, "Basilisk", `http://basilisk.fr`.

[43] Fuster, D., and Popinet, S., 2018, "An all-Mach method for the simulation of bubble dynamics problems in the presence of surface tension", *Journal of Computational Physics*, Vol. 374, pp. 752–768.

[44] Weymouth, G. D., and Yue, D. K.-P., 2010, "Conservative volume-of-fluid method for free-surface simulations on cartesian-grids", *Journal of Computational Physics*, Vol. 229 (8), pp. 2853–2865.

[45] Rudman, M., 1998, "A volume-tracking method for incompressible multifluid flows with large density variations", *International Journal for numerical methods in fluids*, Vol. 28 (2), pp. 357–378.

[46] Bell, J. B., Colella, P., and Glaz, H. M., 1989, "A second-order projection method for the incompressible Navier-Stokes equations", *Journal of computational physics*, Vol. 85 (2), pp. 257–283.

[47] Brackbill, J. U., Kothe, D. B., and Zemach, C., 1992, "A continuum method for modeling surface tension", *Journal of computational physics*, Vol. 100 (2), pp. 335–354.

[48] Popinet, S., 2015, "A quadtree-adaptive multigrid solver for the Serre–Green–Naghdi equations", *Journal of Computational Physics*, Vol. 302, pp. 336–358.

[49] Van Hooft, J. A., Popinet, S., Van Heerwaarden, C. C., Van der Linden, S. J., de Roode, S. R., and Van de Wiel, B. J., 2018, "Towards adaptive grids for atmospheric boundary-layer simulations", *Boundary-layer meteorology*, Vol. 167 (3), pp. 421–443.

[50] Wu, S., Zhang, J., Xiao, Q., and Ni, M.-J., 2021, "Comparison of two interfacial flow solvers: Specific case of a single droplet impacting onto a deep pool", *Computers & Mathematics with Applications*, Vol. 81, pp. 664–678.

[51] Fedorchenko, A. I., and Wang, A.-B., 2004, "On some common features of drop impact on liquid surfaces", *Physics of Fluids*, Vol. 16 (5), pp. 1349–1365.